Supplementary Information for:

Dzyaloshinskii-Moriya interaction engineering for field-free ultra-small skyrmions in alkali-functionalized monolayer Cr_2Te_3

Yaoyuan Wang, [a] Yonglong Ga, [b] Yingmei Zhu, [c] Jiawei Jiang, [b] Hongxin Yang, [†b] Jun Ouyang, [‡a] and Long You[*a]

[a] *School of Integrated Circuits, Huazhong University of Science and Technology, Wuhan 430074, China*
[b] *Center for Quantum Matter, School of Physics, Zhejiang University, Hangzhou 310058, China*
[c] *State Key Laboratory of Spintronics Devices and Technologies, Hangzhou,311305,China*

[*]Corresponding author: lyou@hust.edu.cn

[‡]Corresponding author: oyj@hust.edu.cn

[†]Corresponding author: hongxin.yang@zju.edu.cn

Figures and Figure captions:

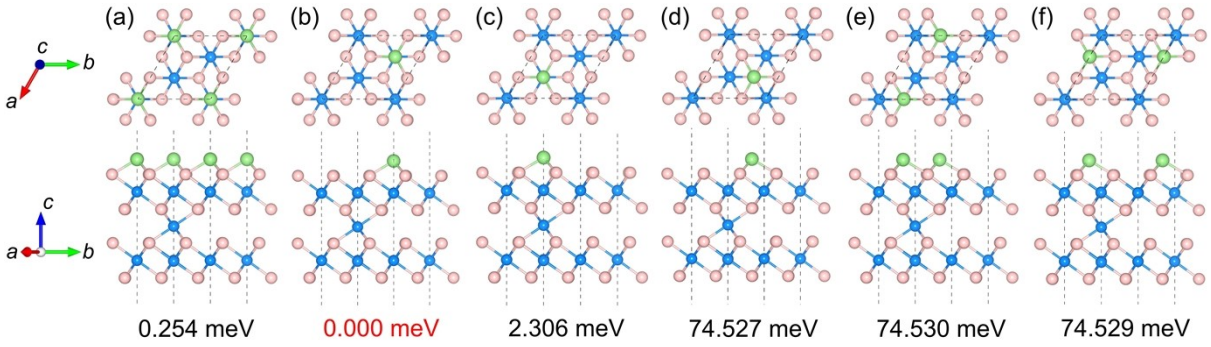

Fig. S1. (a)-(f) Top and side views of six different high-symmetry structures of 33.3% alkali-adsorbed monolayer Cr_2Te_3, where configuration (b) is the most stable.

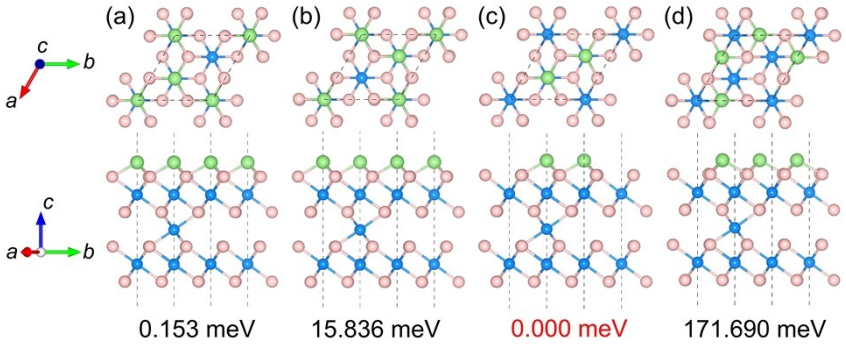

Fig. S2. (a)-(d) Top and side views of four different high-symmetry structures of 66.7% alkali-adsorbed monolayer Cr_2Te_3, where configuration (c) is the most stable.

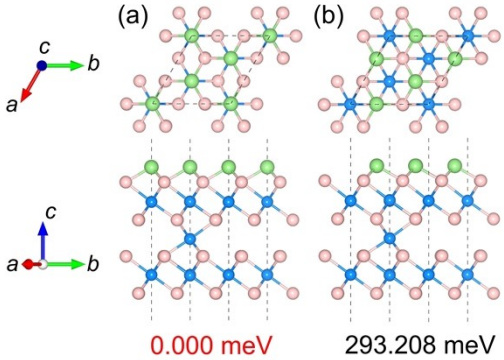

Fig. S3. (a)(b) Top and side views of two different high-symmetry structures of 100% alkali-adsorbed monolayer Cr_2Te_3, where configuration (a) is the most stable.

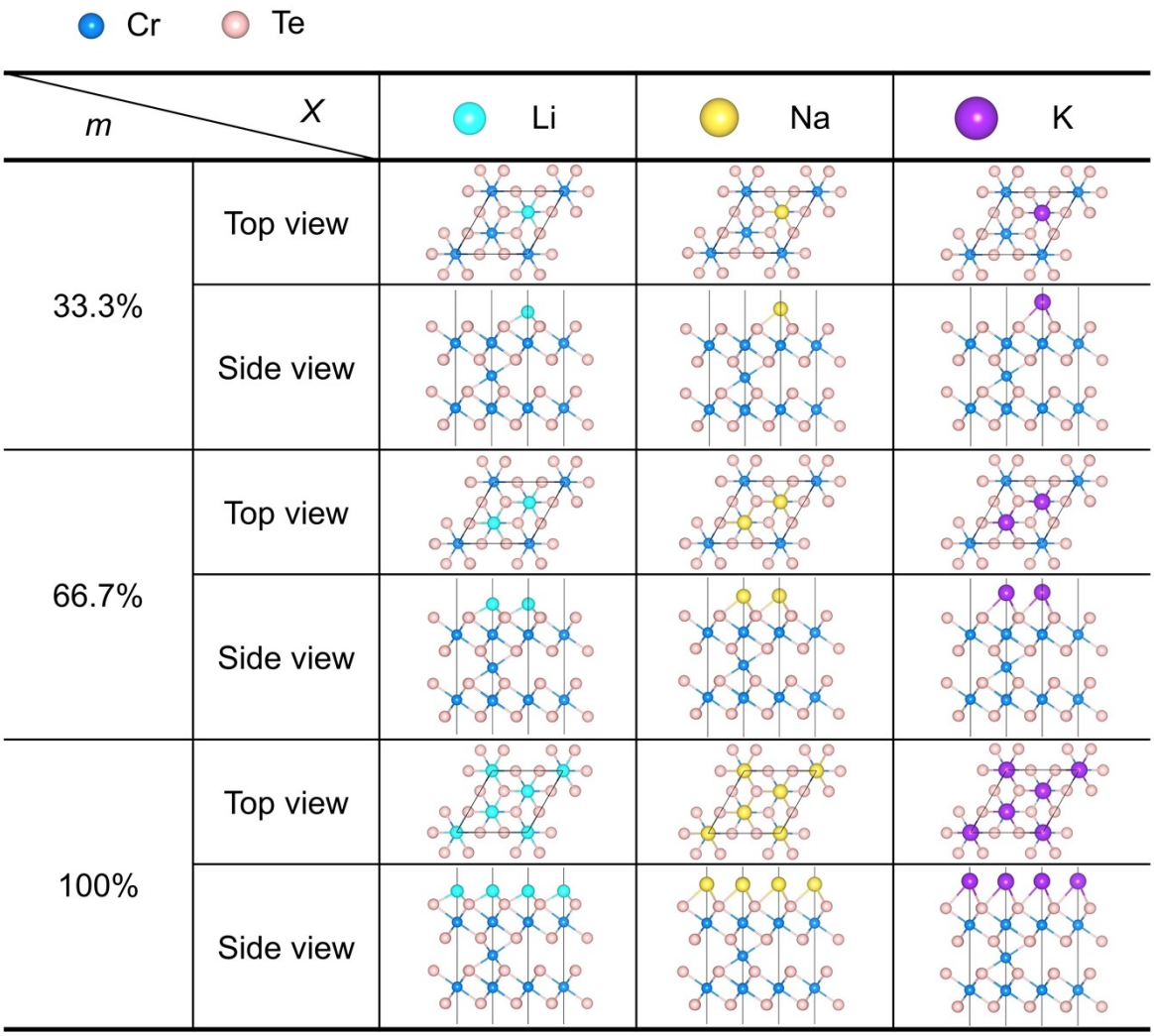

Fig. S4. Tested the most stable structures of alkali-based Cr_2Te_3, where " *X* " represents different types of adsorbed atoms, *X* = Li, Na, K, " *m* " represents different adsorption ratios, *m* = 33.3%, 66.7%, 100%.

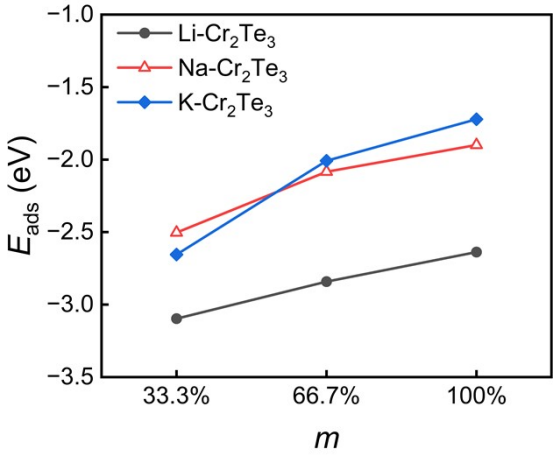

Fig. S5. Calculated average adsorption energy (E_{ads}) per adatom for Li, Na, and K on the Cr_2Te_3 monolayer as a function of the adsorption ratio (m).

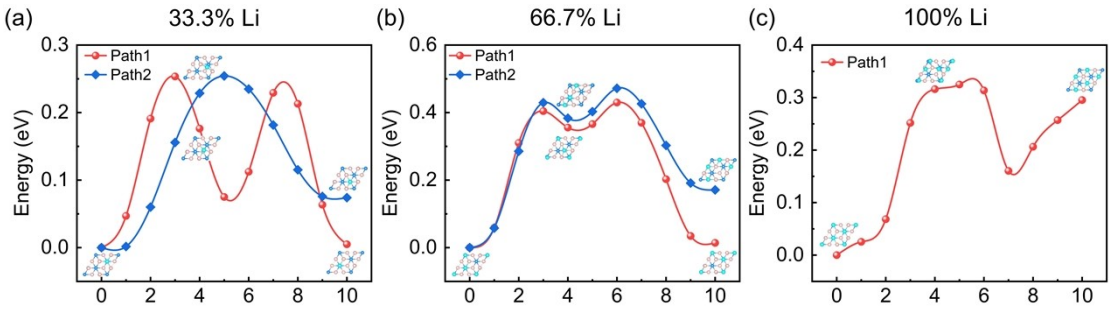

Fig. S6. Energy profiles for Li diffusion on the Cr_2Te_3 monolayer calculated using the CI-NEB method at different adsorption ratios m: (a) m = 33.3%, (b) m = 66.7%, and (c) m = 100%. The red and blue curves represent different diffusion pathways, taking into account structural symmetry. The insets illustrate the corresponding atomic configurations at the initial, transition, and final states.

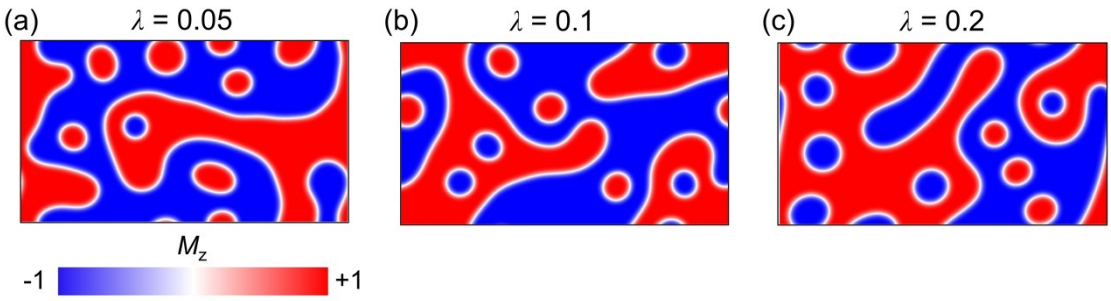

Fig. S7. Effect of the Gilbert damping parameter (λ) on the relaxed magnetic spin textures of 100 × 60 nm^2 33.3%Li-Cr_2Te_3.

In our atomistic spin dynamics simulations, a relatively large $\lambda = 0.2$ is utilized. Physically, 2D heavy-chalcogenide magnets inherently exhibit enhanced effective damping due to the strong spin-orbit coupling from heavy Te atoms, [1] consistent with recent experimental observations in related 2D tellurides. [2] Computationally, this is a standard numerical practice to accelerate convergence to the global energy minimum. [3] As demonstrated in Fig. S7, the final relaxed magnetic ground states (including skyrmion morphology and spatial distribution) remain virtually identical regardless of the chosen λ (0.05, 0.1, or 0.2), explicitly confirming that our numerical choice does not alter the physical results.

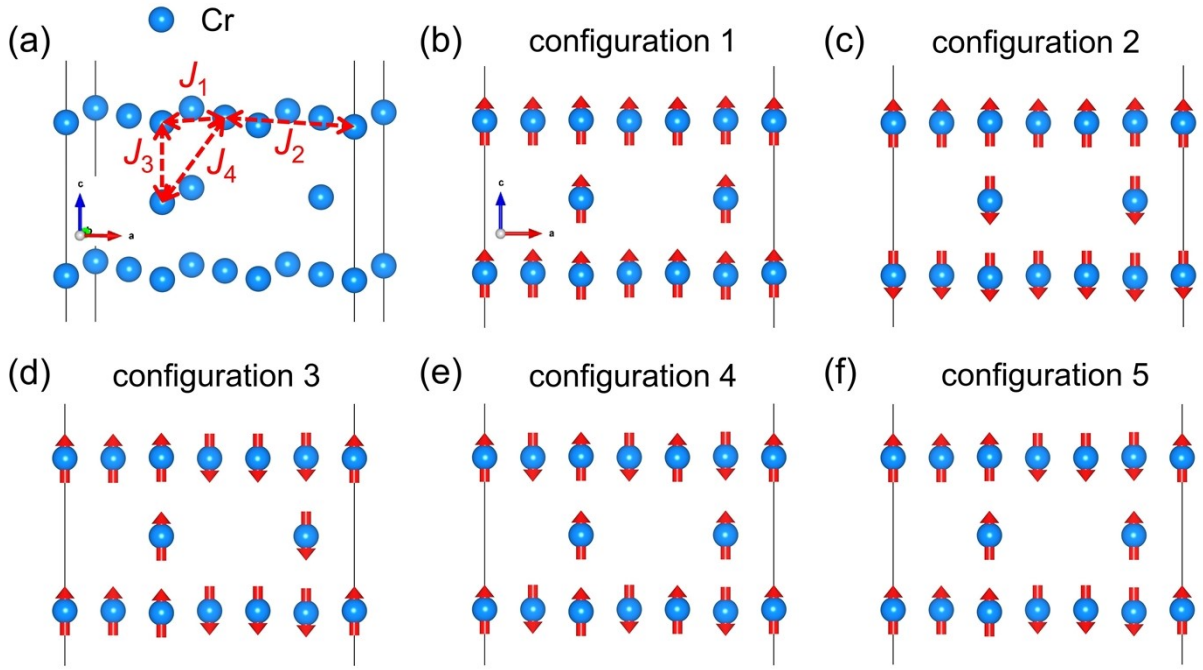

Fig. S8. (a) A $\sqrt{3}\times1\times1$ supercell of alkali-based Cr_2Te_3 is constructed to extract the intralayer nearest neighbor (NN), next-nearest neighbor (NNN), and interlayer NN, NNN exchange interaction constants J_1, J_2 and J_3, J_4. (b)-(f) Schematic presentation of five magnetic configurations to determine J_1 , J_2 , J_3 and J_4 . Note that only the magnetic Cr atoms are depicted for clarity.

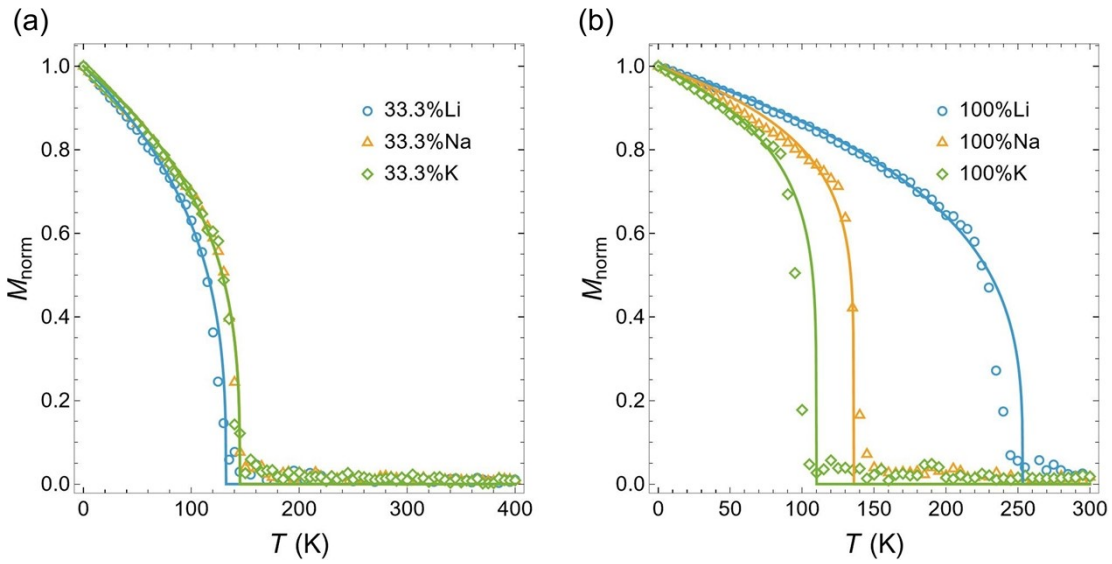

Fig. S9. The Monte Carlo simulations of normalized magnetization (M_{norm}) as a function of temperature (T) for the 33.3% and 100% X-Cr_2Te_3.

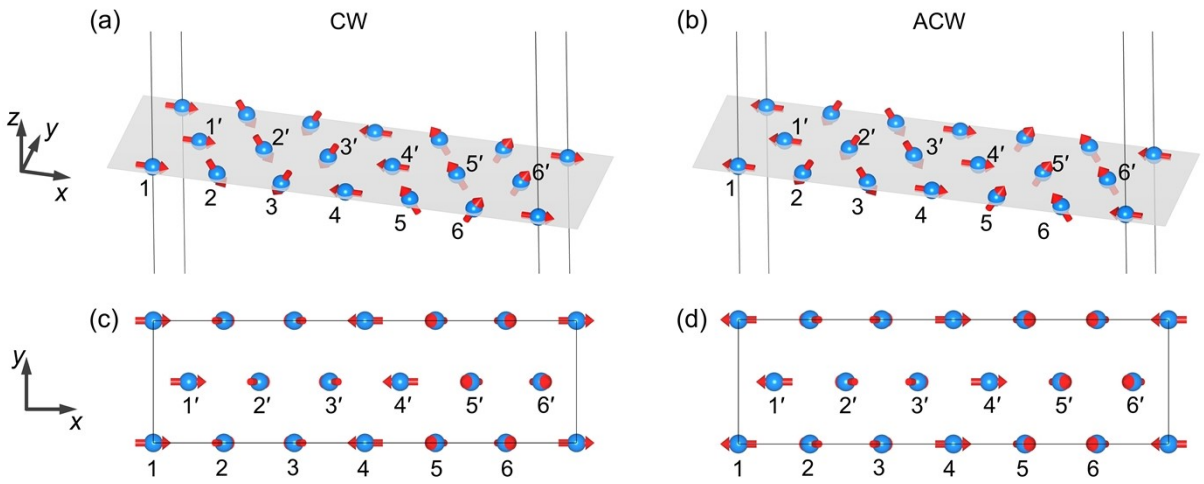

Fig. S10. Two spin spiral configurations of the top or bottom layer (k = 1 or 3) for $2\sqrt{3}\times1\times1$ mX-Cr_2Te_3 supercell used to DMI calculations, including (a)(c) clockwise(CW) and (b)(d) anti-clockwise(ACW). Only the magnetic Cr atoms are shown, and the others are hidden.

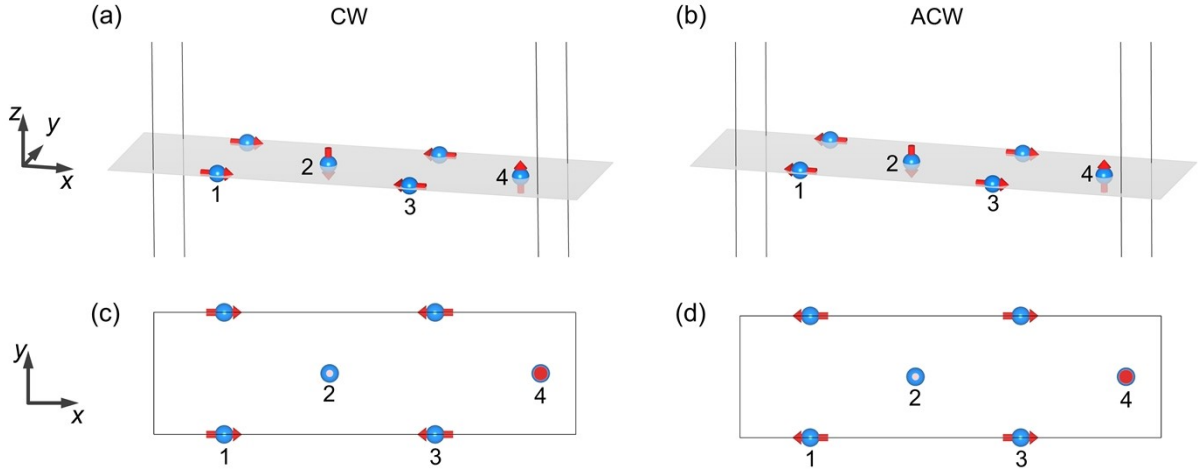

Fig. S11. Two spin spiral configurations of the middle layer (k = 2) for $2\sqrt{3}\times1\times1$ mX-Cr_2Te_3 supercell used to DMI calculations, including (a)(c) clockwise(CW) and (b)(d) anti-clockwise(ACW). Only the magnetic Cr atoms are shown, and the others are hidden.

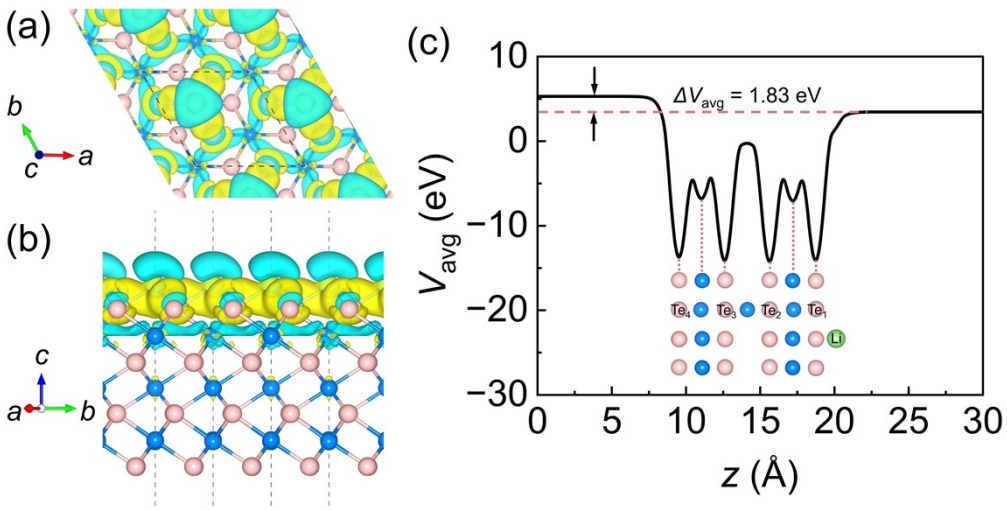

Fig. S12. (a, b) Top and side views of the charge density difference (CDD) of the 33.3%Li-Cr_2Te_3. The yellow and cyan isosurfaces represent electron accumulation and depletion, respectively, indicating massive charge transfer and local hybridization at the top interface. (c) The Planar Average Potential (V_{avg}) along the out-of-plane z-direction for the 33.3%Li-Cr_2Te_3.

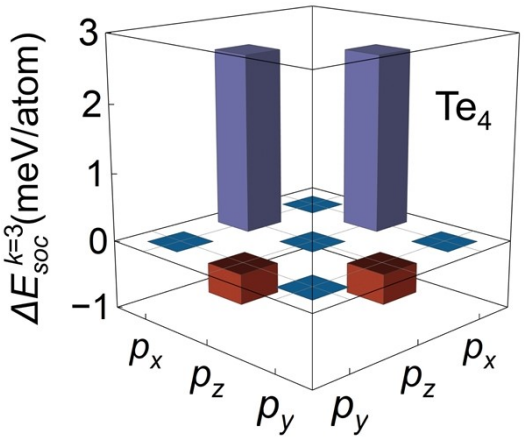

Fig. S13. Orbital-resolved localization of d^3-associated SOC energy ($\Delta E_{soc}^{k=3}$) matrix elements from the bottom-layer Te_4 atom in the 33.3%Li-Cr_2Te_3. The results highlight that the DMI (d^3) is predominantly governed by the coupling between the p_z and p_x orbitals of Te_4.

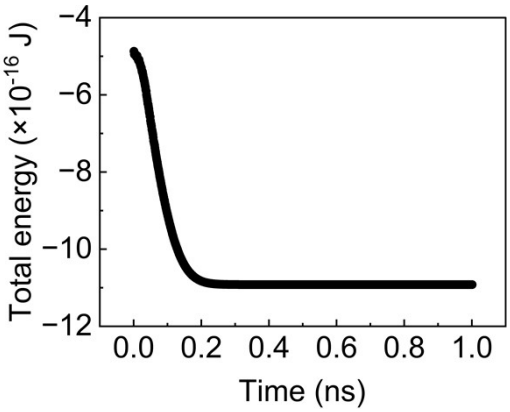

Fig. S14. Calculated total energy as a function of time for the 33.3%K-Cr_2Te_3 system during a 1.0 ns spin dynamics simulation. Following a rapid initial relaxation within 0.2 ns, the energy maintains a constant plateau, confirming that the ultra-small skyrmions are perfectly preserved within a deep local energy minimum.

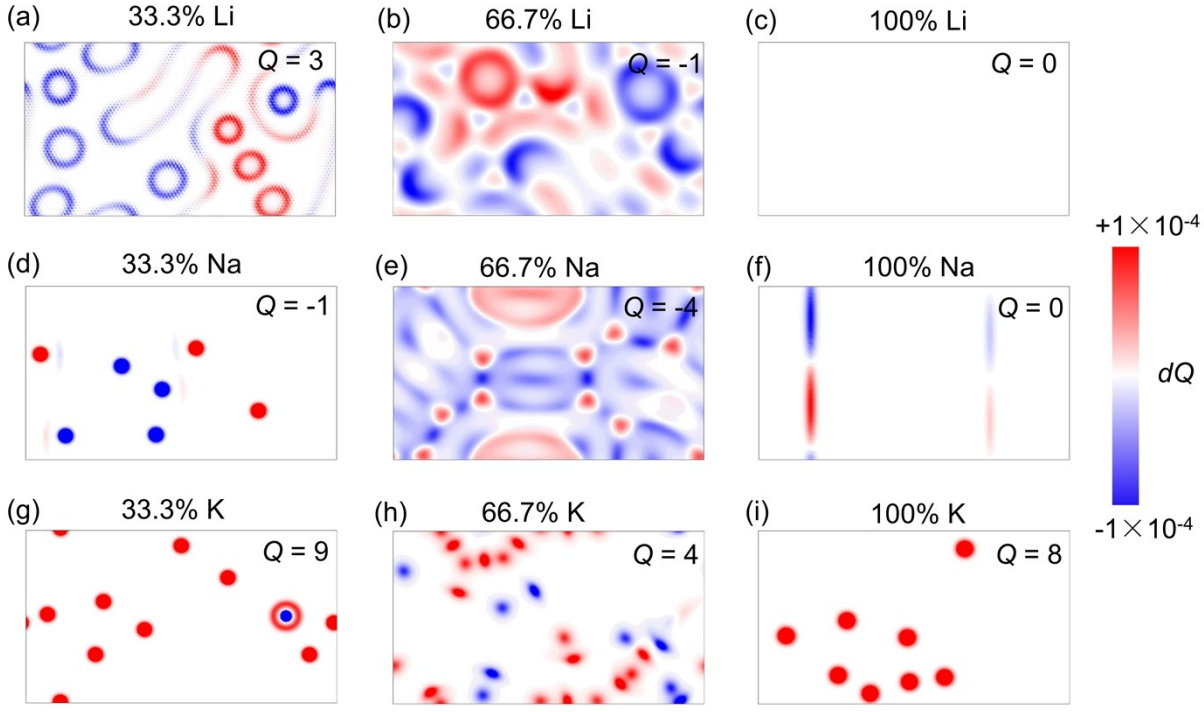

Fig. S15. The distribution of topological charge density (dQ) for 100 nm × 60 nm mX-Cr_2Te_3 in real space. Red (blue) indicates positive (negative) dQ, while white denotes zero topological charge density. The total topological charge Q is labeled in the top-right corner of each panel.

Table S1.The summarized Te-*X* (*X* = Li, Na, K) bond length *l* for alkali-based Cr_2Te_3. The unit is Å.

Absorbed ratio *m*	Te-*X* bond length *l*		
	X = Li	*X* = Na	*X* = K
33.3%	2.670	3.005	3.315
66.7%	2.644	2.983	3.329
100%	2.600	3.073	3.404

References

1 V. Kamberský, *Phys. Rev. B*, 2007, **76**, 134416.

2 J. Zhang, Z. Wang, Z. Li, T. Li, S. Liu, J. Zhang, R.-J. Zhang, Q. Jin, Z. Shi, Y. Liu, Z. Sheng and Z. Zhang, *Nano Lett.*, 2024, **24**, 12204–12210.

3 R. F. L. Evans, W. J. Fan, P. Chureemart, T. A. Ostler, M. O. A. Ellis and R. W. Chantrell, *J. Phys.: Condens. Matter*, 2014, **26**, 103202.